

10. M. Ashburner, H. L. Carson, J. N. Thompson, *The Genetics and Biology of Drosophila* (Academic Press, San Diego, CA, 1997).

11. Materials and methods are available as supporting material on Science Online.

12. The Jackson Laboratory, [www.jaxmice.jax.org/info/consonic.html](http://www.jaxmice.jax.org/info/consonic.html).

13. R. S. Surwit et al., *Metabolism* **44**, 645 (1995).

14. G. A. Brockmann, M. R. Bevova, *Trends Genet.* **18**, 367 (2002).

15. J. N. Crawley et al., *Psychopharmacology (Berl.)* **132**, 107 (1997).

16. J. N. Crawley, *What's Wrong With My Mouse? Behavioral Phenotyping of Transgenic and Knockout Mice* (Wiley-Liss, New York, 2000).

17. C. R. Scriver et al., *The Metabolic and Molecular Bases of Inherited Disease*. C. R. Scriver, Ed. (McGraw-Hill, New York, ed. 8, 2001), vol. II.

18. E. Lander, L. Kruglyak, *Nature Genet.* **11**, 241 (1995).

19. J. Flint et al., *Science* **269**, 1432 (1995).

20. H. K. Gershenfeld et al., *Behav. Genet.* **27**, 201 (1997).

21. M. G. Turri, N. D. Henderson, J. C. DeFries, J. Flint, *Genetics* **158**, 1217 (2001).

22. S. Zhang, H. K. Gershenfeld, *Obes. Res.* **11**, 828 (2003).

23. J. K. Belknap, *Mamm. Genome* **14**, 723 (2003).

24. CHORI-27 Mus musculus A/J BAC Library, <http://bacpac.chori.org/mouse27.htm>.

25. A. W. Cowley Jr. et al., *Hypertension* **37**, 456 (2001).

26. R. J. Roman et al., *Cold Spring Harb. Symp. Quant. Biol.* **67**, 309 (2002).

27. This work was supported by NIH NCRR grant RR12305, NICHD grant HD07518, and NIGMS grant GM07250.

**Supporting Online Material**

[www.sciencemag.org/cgi/content/full/1093139/DC1](http://www.sciencemag.org/cgi/content/full/1093139/DC1)  
 Materials and Methods  
 SOM Text  
 Figs. S1 and S2  
 Table S1  
 References

30 October 2003; accepted 9 March 2004  
 Published online 18 March 2004; 10.1126/science.  
 1093139  
 Include this information when citing this paper.

# ABAD Directly Links Aβ to Mitochondrial Toxicity in Alzheimer's Disease

Joyce W. Lustbader,<sup>1\*</sup> Maurizio Cirilli,<sup>3\*†</sup> Chang Lin,<sup>2\*‡</sup>  
 Hong Wei Xu,<sup>2,4</sup> Kazuhiro Takuma,<sup>2§</sup> Ning Wang,<sup>2‡</sup>  
 Casper Caspersen,<sup>2</sup> Xi Chen,<sup>5</sup> Susan Pollak,<sup>1</sup> Michael Chaney,<sup>2</sup>  
 Fabrizio Trinchese,<sup>6</sup> Shumin Liu,<sup>6</sup> Frank Gunn-Moore,<sup>7</sup>  
 Lih-Fen Lue,<sup>8</sup> Douglas G. Walker,<sup>8</sup> Periannan Kuppusamy,<sup>9</sup>  
 Zay L. Zewier,<sup>9</sup> Ottavio Arancio,<sup>6</sup> David Stern,<sup>10</sup>  
 Shirley ShiDu Yan,<sup>2||</sup> Hao Wu<sup>3||¶</sup>

Mitochondrial dysfunction is a hallmark of β-amyloid (Aβ)-induced neuronal toxicity in Alzheimer's disease (AD). Here, we demonstrate that Aβ-binding alcohol dehydrogenase (ABAD) is a direct molecular link from Aβ to mitochondrial toxicity. Aβ interacts with ABAD in the mitochondria of AD patients and transgenic mice. The crystal structure of Aβ-bound ABAD shows substantial deformation of the active site that prevents nicotinamide adenine dinucleotide (NAD) binding. An ABAD peptide specifically inhibits ABAD-Aβ interaction and suppresses Aβ-induced apoptosis and free-radical generation in neurons. Transgenic mice overexpressing ABAD in an Aβ-rich environment manifest exaggerated neuronal oxidative stress and impaired memory. These data suggest that the ABAD-Aβ interaction may be a therapeutic target in AD.

Human ABAD (also known as ERAB and HSD-10) was the only protein identified from four positive clones that bound Aβ in a yeast two-hybrid screen against human brain and HeLa cDNA libraries (1, 2). Biochemical characterization has established that the interaction between ABAD and Aβ is highly specific and starts to occur at nanomolar concentrations. At micromolar concentrations, Aβ, likely in its oligomeric form, inhibits ABAD enzymatic activity (1, 3, 4). ABAD appears to have an essential physiological role in mitochondria (1, 3), and mutational inactivation of *Drosophila* ABAD (*scully*) resulted in a lethal phenotype (5). ABAD is up-regulated in affected neurons in AD (1) (fig. S1), and coexpression of ABAD with mutant amyloid precursor protein (mAPP) exacerbates Aβ-induced cellular oxidant stress and cell death (1, 3). Thus, we speculated that the interaction of Aβ with ABAD might induce mitochondrial dysfunction.

However, because it had not been established that intracellular Aβ can access mitochondria, it was essential to determine whether ABAD and Aβ interact in pathophysiologically relevant settings. To address this directly, we detected ABAD-Aβ complex in AD brains by immunoprecipitating cortical protein extracts with anti-Aβ and then by immunoblotting with anti-ABAD immunoglobulin G (IgG) [Fig. 1A and supporting online material (SOM) text S1]. Age-matched nondemented brain displayed very little ABAD-Aβ complex. Because cellular and mitochondrial integrity may start to deteriorate soon after death, allowing nonphysiological interactions to occur, we isolated mitochondria from the cerebral cortex of 12-month-old mice expressing mAPP (6), ABAD (7), or both, driven by the platelet-derived growth factor B-chain promoter (SOM text S2 and S3). The purity of mitochondrial preparations was confirmed by the enrichment of cyto-

chrome c oxidase IV (Cox IV), and the relative absence of lysosomal (cathepsin D) and endoplasmic reticulum [protein disulfide isomerase (PDI)] markers (Fig. 1B). ABAD-Aβ complex was evident in the mitochondria of both transgenic (Tg) mAPP and Tg mAPP/ABAD mice (fig. S2A). Similar bands were only present at very low levels in samples from age- and strain-matched non-Tg littermates or when non-immune IgG replaced specific antibodies.

We used confocal microscopy to confirm mitochondrial colocalization and interaction of ABAD and Aβ. In the cerebral cortex of AD patients, images of anti-ABAD (red) and anti-Aβ (green), detecting endogenous ABAD and Aβ, extensively colocalize (Fig. 1C). Similarly, in the cerebral cortex of Tg mAPP/ABAD mice, there is extensive overlap of immunoreactive ABAD and Aβ (fig. S2B). Because ABAD

<sup>1</sup>Center for Reproductive Sciences and Department of Obstetrics and Gynecology, <sup>2</sup>Departments of Pathology and Surgery, College of Physicians and Surgeons, Columbia University, 630 West 168th Street, New York, NY 10032, USA. <sup>3</sup>Department of Biochemistry, Weill Medical College of Cornell University, 1300 York Avenue, New York, NY 10021, USA. <sup>4</sup>Department of Immunology, Harbin Medical University, Harbin 150086, China. <sup>5</sup>Department of Neurology, New York University, New York, NY 10003, USA. <sup>6</sup>Dementia Research Center, Nathan Kline Institute and Department of Psychiatry, Physiology and Neuroscience, New York University, New York, NY 10016, USA. <sup>7</sup>School of Biology, Bute Medical Building, University of St. Andrews, St. Andrews KY16 9TS, Scotland, UK. <sup>8</sup>Sun Health Research Institute, Sun City, AZ 85351, USA. <sup>9</sup>David Heart and Lung Research Institute, Ohio State University, Columbus, OH 43210, USA. <sup>10</sup>Dean's Office, Medical College of Georgia, Augusta, GA 30912, USA.

\*These authors contributed equally to the work.  
 †Present address: Institute of Neurobiology and Molecular Medicine—Italian National Council of Research, Via del Fosso del Cavaliere, 100, 00133 Rome, Italy.  
 ‡Present address: Departments of Otolaryngology and Neurology, First Affiliated Hospital, Fujian Medical University, Fujian 350005, China.  
 §Present address: Department of Analytical Chemistry, Faculty of Pharmaceutical Science, Kobe Gakuin University, Kobe 651-2180, Japan.  
 ||These authors contributed equally to the work.  
 ¶To whom correspondence should be addressed. E-mail: haowu@med.cornell.edu (H.W.); sdy1@columbia.edu (S.S.Y.)

is mainly localized to mitochondria, as shown by the overlap of anti-ABAD (green) and anti-voltage-dependent anion channel (VDAC) (red) images (Fig. 1D), these data demonstrate that A $\beta$  is also present in the mitochondria of AD patients. Immunogold electron microscopy with gold-conjugated antibody systems provided further evidence for the presence of ABAD and A $\beta$  within mitochondria (18-nm gold particles for ABAD and 12-nm gold particles for A $\beta$ ). The two different sizes of gold particles are concentrated in the mitochondria of brains from a patient with AD (Fig. 1E) and from Tg mAPP/ABAD mice (fig. S2C). Taken together, these microscopic and immunoprecipitation data demonstrate the formation of ABAD-A $\beta$  complex within mitochondria in vivo.

To determine the structural basis of the ABAD-A $\beta$  interaction, we crystallized and determined the structure of human ABAD in the presence of a molar excess of NAD and A $\beta$  at 2.3 Å resolution (Fig. 2A, table S1, and SOM text S4). Unexpectedly, NAD is not bound to ABAD in the crystal structure. Under the crystallization condition, A $\beta$  inhibits

ABAD activity, but in the absence of A $\beta$ , ABAD displays normal activity. This suggests that A $\beta$  prevents NAD binding in the crystal structure, which may be the molecular basis for its inhibition of ABAD activity.

SDS-polyacrylamide gel electrophoresis and N-terminal sequencing of washed and dissolved crystals showed that both ABAD and A $\beta$  are present in the crystals (fig. S3A). However, no electron density is observed for A $\beta$ , suggesting that A $\beta$  itself and the region of ABAD that binds to A $\beta$  must be disordered in the crystal. To exclude the possibility that A $\beta$  interacts with ABAD nonspecifically, we performed additional experiments, which showed that other amyloid species such as a prion-derived peptide and amylin did not bind to ABAD. In addition, A $\beta$  residues 1 to 42 [A $\beta$ (1-42)], A $\beta$ (1-40), and A $\beta$ (1-20) demonstrated dose-dependent binding, whereas A $\beta$ (25-35) showed no specific binding (table S2).

The comparison of the A $\beta$ -bound ABAD structure with the rat ABAD structure in complex with NAD (8) and the human ABAD structure in complex with NAD and a small-molecule inhibitor (9) shows that the

A $\beta$ -bound ABAD displays substantial distortion of the NAD-binding pocket and the catalytic triad (Fig. 2, B and C, and fig. S3B). The majority of the L<sub>D</sub> loop, the beginning of the following  $\alpha_D$  helix, and the latter part of the L<sub>F</sub> loop of human ABAD are disordered. Although the L<sub>E</sub> loop is ordered, the conformation of the loop and the beginning of the following  $\alpha_E$  helix is markedly different from the structure without A $\beta$ .

In the absence of substrate, the L<sub>F</sub> loop is also disordered in the rat ABAD structure in complex with NAD, whereas the L<sub>D</sub> loop region is well ordered, suggesting that A $\beta$  binding may have influenced the L<sub>D</sub> loop dynamics and conformation. In addition, within the NAD-dependent short-chain dehydrogenase/reductase (SDR) superfamily, the L<sub>D</sub> loop of ABAD from different species contains a unique insertion that is absent in all other SDRs (fig. S3C). Because ABAD is the only SDR that has been observed to bind A $\beta$ , we hypothesize that the L<sub>D</sub> loop may be a recognition site for A $\beta$ .

Inspection of crystal packing showed that the ordered ends of the L<sub>D</sub> loop point into huge interconnected solvent channels with estimated dimensions of 70 Å (Fig. 2D). It is estimated that the ordered part of the crystal only occupies about 30% of the total crystal volume. Sufficient space is therefore available for the disordered loops and the bound A $\beta$ , which could drift freely in the large solvent channels in the crystal to cause disorder or nonspecifically bind and clog the active-site region to inactivate the enzyme.

To test the idea that the L<sub>D</sub> loop is important in A $\beta$  interaction, we performed structure-based mutational analyses (Table 1). Binding studies with A $\beta$  and glutathione *S*-transferase (GST)-ABAD truncation mutants showed that the N-terminal portion

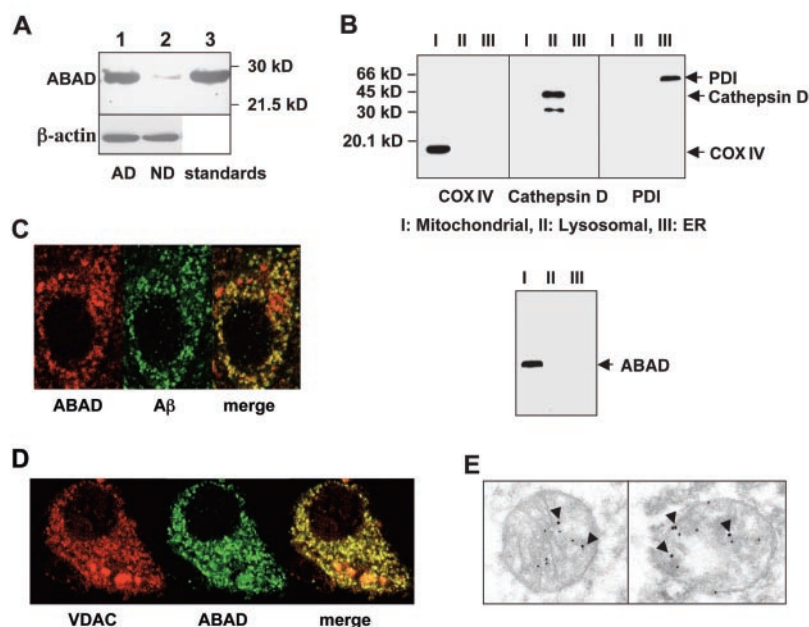


**Fig. 1.** ABAD-A $\beta$  association in AD patients and transgenic mice. **(A)** Coimmunoprecipitation of ABAD and A $\beta$  in AD patient brains. Results shown are representative of the three patients in each group. **(B)** Subcellular fractionation was used to prepare fractions of mouse brain enriched for mitochondrial (fraction I), lysosomal (fraction II), or endoplasmic reticulum (fraction III) constituents. Each fraction (20  $\mu$ g total protein per lane) was immunoblotted with antibodies to Cox IV, cathepsin D, and PDI. Protein loading was identical in each case. Lower panel shows the presence of ABAD in the mitochondrial fraction. **(C)** Colocalization of ABAD and A $\beta$  in cerebral cortex of AD patients (200-fold magnification). **(D)** Mitochondrial localization of ABAD in cerebral cortex of AD patients (200-fold magnification). VDAC was used as a mitochondrial marker. Mouse anti-VDAC (20  $\mu$ g/ml), guinea pig anti-ABAD (10  $\mu$ g/ml), and rabbit anti-A $\beta$  (5  $\mu$ g/ml) IgGs were used in (C) and (D). **(E)** Colocalization of ABAD and A $\beta$  in mitochondria of the brain of a patient with AD with the use of electron microscopy. Double immunogold staining was performed with rabbit anti-A $\beta$  IgG and mouse anti-ABAD IgG followed by goat anti-rabbit IgG conjugated to 12-nm gold particles (for A $\beta$ 1-42) and goat anti-mouse IgG conjugated to 18-nm gold particles (for ABAD). Arrowheads depict gold particles localizing ABAD antigen. The smaller gold particles represent sites of localization of A $\beta$ .

**Table 1.** Mutational studies of ABAD. The binding of <sup>125</sup>I-labeled GST-ABAD or ABAD to immobilized A $\beta$ (1-42) was performed as previously described (7). +, specific binding comparable to that observed with wild-type ABAD; -, no observed specific binding. Numbers in parentheses indicate residue numbers.

ABAD mutations	A $\beta$ Binding
<i>Experiments with ABAD truncations</i>	
GST-ABAD (1-186)	+
GST-ABAD (1-158)	+
GST-ABAD (159-261)	-
<i>Experiments with site-directed ABAD mutations</i>	
G93A	+
S98A, K99A	+
S98A, K99A, T100A, Y101A	-
S98A, K99A, Y101A	-
N102A	+
N102A, L103A	+
T108A, H109A, T110A	-
V156A	+
Q162A	+

of ABAD (residues 1 to 158) is responsible for A $\beta$  interaction. Site-directed mutagenesis within and beyond the disordered L<sub>D</sub> loop region (residues 95 to 113) specifically located two stretches of ABAD residues important for A $\beta$  binding: residues S<sup>98</sup> to Y<sup>101</sup> (10) and residues T<sup>108</sup> to T<sup>110</sup>. An ABAD mutant bearing Ser<sup>98</sup>→Ala<sup>98</sup> (S98A), K99A, and Y101A mutations exhibited no specific interaction to A $\beta$  in a surface plasmon resonance experiment, although wild-type ABAD displayed dose-dependent interaction with A $\beta$  (Fig. 3A).

To determine whether the L<sub>D</sub> loop is sufficient for A $\beta$  interaction, we synthesized a peptide encompassing this region (residues 92 to 120) of human ABAD [termed ABAD decoy peptide (ABAD-DP)] and used surface plasmon resonance to test its ability to inhibit the interaction of intact ABAD with A $\beta$  (Fig. 3B and SOM text S5). ABAD-DP inhibited binding of A $\beta$ (1–40) (fig. S4A) and A $\beta$ (1–42) (Fig. 3B) to immobilized intact ABAD with inhibitory constants of 4.9 and 1.7  $\mu$ M, respectively. In contrast, a peptide of the reverse sequence [residues 120 to 92, termed ABAD reversed peptide (ABAD-RP)] was completely inactive. These competitive binding studies confirmed that the L<sub>D</sub> region alone could mediate A $\beta$  binding, although it may not be the exclusive site.

To develop a specific inhibitor of the ABAD-A $\beta$  interaction in cultured neurons, we added the cell-membrane transduction domain of the human immunodeficiency virus-1 (HIV-1) Tat protein (11, 12) to ABAD-DP and ABAD-RP (thereby enabling the peptides to cross cell membranes). We used cytochrome c release from mitochondria as a marker of A $\beta$ -induced cellular stress and apoptosis (SOM text S6). Whereas cultured wild-type cortical neurons exposed to A $\beta$ (1–42) suffered loss of cytochrome c from the mitochondrial or membrane fraction to the cytosol fraction, preincubation of the cells with ABAD-DP but not with ABAD-RP largely prevented A $\beta$ -induced cytochrome c release (Fig. 3C). Similarly, ABAD-DP protected against A $\beta$ -induced mitochondrial cytochrome c release in neurons from Tg ABAD mice, although these neurons displayed enhanced cytochrome c release compared with that of non-Tg mice. Furthermore, pretreatment with ABAD-DP but not with ABAD-RP markedly reduced spontaneous loss of cytochrome c from the mitochondrial/membrane fraction of cultured neurons derived from Tg mAPP/ABAD mice.

The protective effects of cell-permeable ABAD-DP are consistent with the hypothesis that the ABAD-A $\beta$  interaction causes mitochondrial stress and apoptosis. Because mitochondria are the principal sites of generation of reactive oxygen species (ROS) under physiologic conditions, and

A $\beta$  is known to trigger oxidative stress, we tested whether the protection from A $\beta$ -induced cytotoxicity by ABAD-DP is accompanied by an attenuated generation of ROS (SOM text S7). Cultured neurons loaded with a probe for ROS, dichlorofluorescein diacetate (DCFDA), demonstrated fluorescence on exposure to A $\beta$ , a phenomenon accentuated in neurons from Tg ABAD mice compared with those of non-Tg littermates (fig. S4B). Pretreatment with ABAD-DP virtually completely suppressed fluorescence in DCFDA-loaded and A $\beta$ -exposed neurons from both non-Tg and Tg ABAD animals (fig. S4B). In contrast, there was no effect exerted by ABAD-RP. Furthermore, spontaneous generation of ROS by cultured neurons from Tg mAPP/ABAD mice was suppressed by pretreatment with ABAD-DP but not ABAD-RP (Fig. 3D). Linkage between A $\beta$ -ABAD-induced generation of ROS and subsequent

DNA fragmentation (Fig. 3E) and lactate dehydrogenase (LDH) release (fig. S4D) was shown in cultured neurons from Tg mAPP/ABAD mice. Similarly, cultured neurons from Tg ABAD mice exposed to A $\beta$  display subsequent DNA fragmentation (fig. S4C) and LDH release (fig. S4D). In each case, pretreatment with ABAD-DP but not ABAD-RP attenuated cytotoxicity.

If the above results in cell culture could be extrapolated to in vivo settings, then mice overexpressing ABAD in an A $\beta$ -rich environment (i.e., Tg mAPP/ABAD mice) might exhibit exaggerated oxidative stress and elevated generation of ROS. Electron paramagnetic spin resonance (EPR) spectroscopy (SOM text S8) was used to measure the level of ROS in intact frozen brain at 77 K (Fig. 4A). Notably higher amounts of radicals, as shown by the sharp peak at 3410 G, were observed in the Tg mAPP/ABAD mouse brains, in comparison with brains from non-

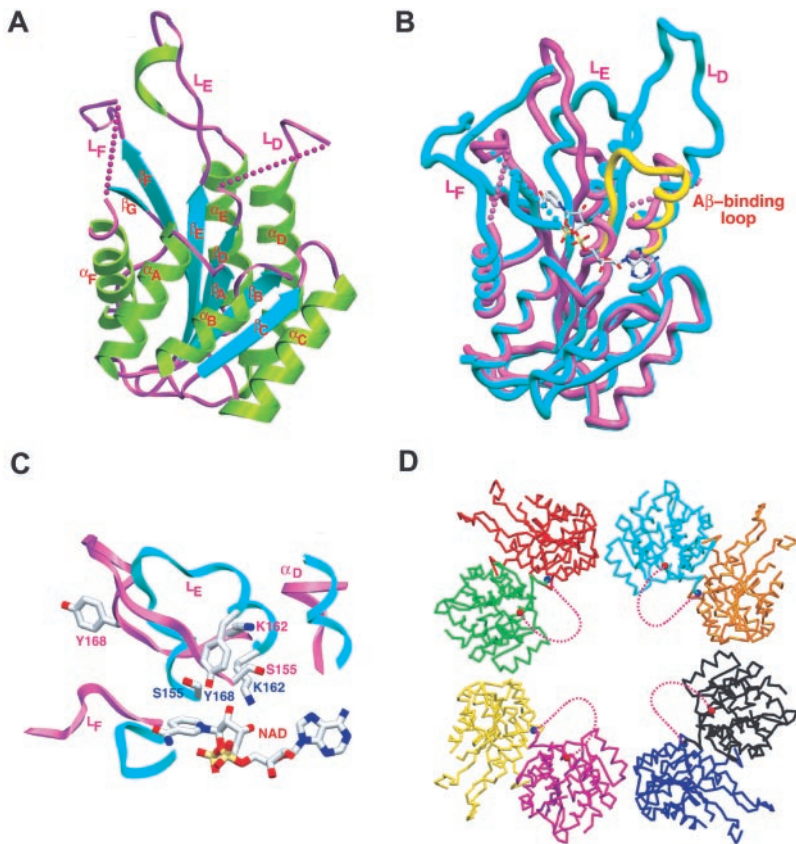


**Fig. 2.** Crystal structure of A $\beta$ -bound human ABAD. (A) A ribbon diagram with labeled secondary structures and the L<sub>D</sub>, L<sub>E</sub>, and L<sub>F</sub> loops. Helices are shown in green,  $\beta$  strands are shown in blue, and loops are shown in pink. Disordered regions are shown by dotted lines. (B) Superposition of A $\beta$ -bound human ABAD (pink) and rat ABAD in complex with NAD (blue). The L<sub>D</sub> loop of 3 $\alpha$ -hydroxysteroid dehydrogenase (3 $\alpha$ -HSD) (PDB code 1FJH) is shown in yellow. NAD is shown as a stick model with gray for carbon atoms, red for oxygen atoms, blue for nitrogen atoms, and yellow for phosphate atoms. The proposed A $\beta$ -binding loop is indicated. (C) Superposition of the active sites of A $\beta$ -bound human ABAD (pink) and rat ABAD (blue), showing distortion of the NAD binding site and the catalytic triad S<sup>155</sup>, K<sup>162</sup>, and Y<sup>168</sup>. Colors are the same as in (B). (D) A section of the crystal packing interactions, showing the large solvent channels. Each ABAD molecule is shown in a different color. The ordered ends of the L<sub>D</sub> loop, residues 94 and 114, are marked as red and blue balls, respectively, and the hypothetical loops are shown in pink as dotted lines.

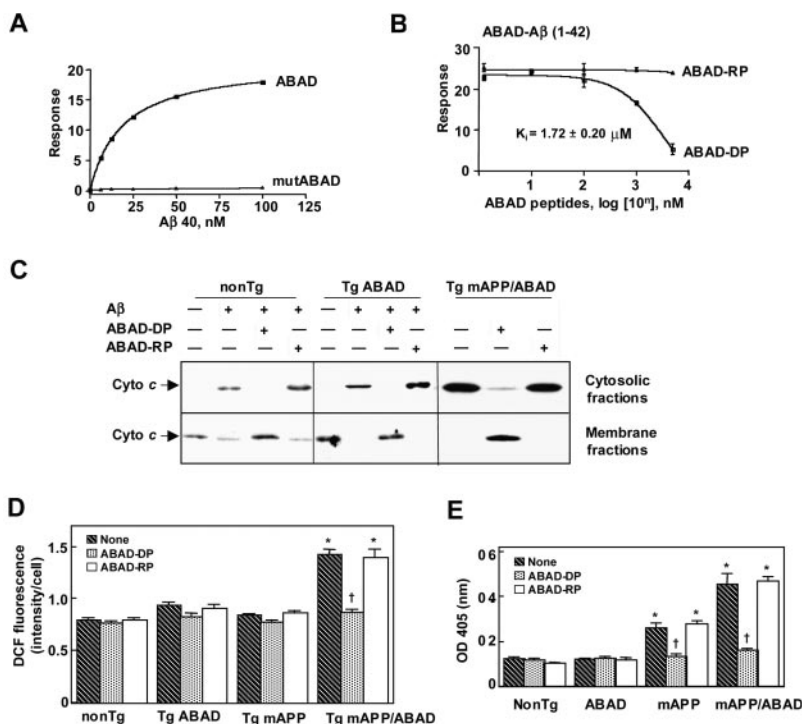


**Fig. 3.** Biochemical and functional effects of ABAD-DP. (A and B) Effect of mutations in the  $L_D$  loop of ABAD on  $A\beta$  binding (A) and inhibition of ABAD- $A\beta$  interaction by ABAD-DP (B), measured by surface plasmon resonance. ABAD was immobilized on the sensor chips; (A) wild-type or mutant (S98A, K99A, Y101A) ABAD was immobilized, and (B) wild-type ABAD was used. In (A), the mobile (injected) phase was  $A\beta(1-40)$ , and in (B), the mobile phase was a mixture of  $A\beta(1-42)$  and either ABAD-DP or ABAD-RP (range of concentrations). (C) Inhibition of  $A\beta$ -induced and spontaneous cytochrome c release from mitochondrial or membrane fraction by ABAD-DP in cultured neurons. (D and E) Inhibition of ROS generation (D) and DNA fragmentation (E) by ABAD-DP. \*,  $P < 0.05$  versus non-Tg cells; †,  $P < 0.05$  versus without ABAD-DP treatment. Error bars show mean  $\pm$  SEM.

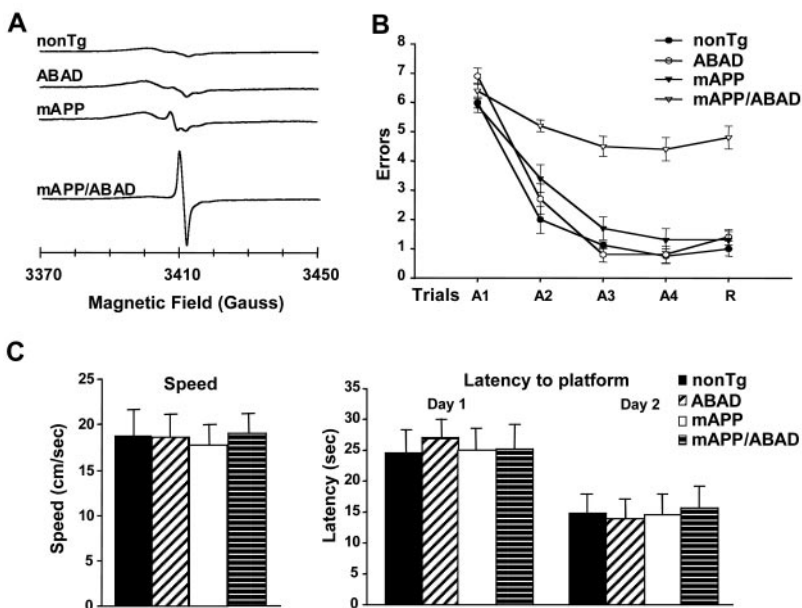


**Fig. 4.** Generation of free radicals and spatial learning and memory deficit in Tg mAPP/ABAD mice. (A) Generation of free radicals in Tg mAPP/ABAD mouse brains, shown by the sharp peak at 3410 G in an EPR spectrum. The amplitude of the spectra for Tg mAPP, Tg ABAD, and non-Tg animals has been increased by 10-fold to display the spectra, which showed only low-level changes. (B) Spatial learning is abnormal in 4.5- to 5-month-old Tg mAPP/ABAD mice tested in the radial-arm water maze ( $P < 0.05$ ;  $N = 7$  to 8). (C) All groups ( $N = 7$  to 8) show similar speed and latency to find a visible platform.

Tg, Tg ABAD, or Tg mAPP mice. It is evident that this species of free radicals, which might be from ascorbyl or the one-electron reduced ubiquinone radical, is generated as a result of higher levels of oxidative stress in Tg mAPP/ABAD (13), compared with those of the other genotypes.

Excessive generation of ROS could result in neuronal dysfunction or, alternatively, could be buffered by protective antioxidant mechanisms without changes in neuronal function. We used the radial-arm water maze test (SOM text S9) to detect hippocampal-dependent learning and memory deficits in Tg mAPP/ABAD mice (14, 15). Young mice (4.5 to 5 months of age) of non-Tg, Tg mAPP, or Tg ABAD transgenic littermates all showed strong learning and memory capacity. As they sought out the new platform location, they averaged less than one to two errors by trials 4 or 5 (Fig. 4B). In contrast, Tg mAPP/ABAD mice failed to learn efficiently and still averaged about four errors by trials 4 or 5 (Fig. 4B), indicative of severe impairment in spatial and temporal memory. Double transgenic expression of ABAD and mAPP did not cause impairment in vision, motor coordination, or motivation. The visible platform test showed that the four genotypes exhibited no difference in their speed of swimming and in their latencies to find the platform (Fig. 4C).

Our data demonstrate that ABAD and  $A\beta$  directly interact in mitochondria in AD, and that this interaction promotes leakage of ROS, mitochondrial dysfunction, and cell death, potentially underlying the mechanism of  $A\beta$ -induced mitochondrial toxicity (16–23). Such events are likely to induce changes in behavior, characterized by exaggerated impairment of hippocampal function in Tg mAPP/ABAD mice. Taken together, these studies establish that  $A\beta$  may exert an important pathogenic role in the mitochondrial compartment through an interaction with ABAD and that inhibition of ABAD- $A\beta$  interaction may provide a new treatment strategy against AD.

**References and Notes**

1. S. D. Yan et al., *Nature* **389**, 689 (1997).
2. K. Beyreuther, C. L. Masters, *Nature* **389**, 677 (1997).
3. S. D. Yan et al., *J. Biol. Chem.* **274**, 2145 (1999).
4. U. C. Oppermann, S. Salim, L. O. Tjernberg, L. Terenius, H. Jornvall, *FEBS Lett.* **451**, 238 (1999).
5. L. Torroja, D. Ortuno-Sahagun, A. Ferrus, B. Hamerle, J. A. Barbas, *J. Cell Biol.* **141**, 1009 (1998).
6. L. Mucke et al., *J. Neurosci.* **20**, 4050 (2000).
7. S. D. Yan et al., *J. Biol. Chem.* **275**, 27100 (2000).
8. A. J. Powell et al., *J. Mol. Biol.* **303**, 311 (2000).
9. M. A. Abreo et al., *U.S. Patent and Trademark Office serial number 931186* (2002), vol. 9.
10. Single-letter abbreviations for the amino acid residues are as follows: A, Ala; C, Cys; D, Asp; E, Glu; F, Phe; G, Gly; H, His; I, Ile; K, Lys; L, Leu; M, Met; N, Asn; P, Pro; Q, Gln; R, Arg; S, Ser; T, Thr; V, Val; W, Trp; and Y, Tyr.
11. M. Aarts et al., *Science* **298**, 846 (2002).

12. M. Becker-Hapak, S. S. McAllister, S. F. Dowdy, *Meth-ods* **24**, 247 (2001).
13. H. P. Grill, J. L. Zweier, P. Kuppusamy, M. L. Weisfeldt, J. T. Flaherty, *J. Am. Coll. Cardiol.* **20**, 1604 (1992).
14. D. Morgan *et al.*, *Nature* **408**, 982 (2000).
15. G. Di Rosa, T. Odrijin, R. A. Nixon, O. Arancio, *J. Mol. Neurosci.* **19**, 135 (2002).
16. R. H. Swerdlow, S. J. Kish, *Int. Rev. Neurobiol.* **53**, 341 (2002).
17. R. Castellani *et al.*, *J. Neurosci. Res.* **70**, 357 (2002).
18. A. D. Cash *et al.*, *Neuroscientist* **8**, 489 (2002).
19. J. P. Blass, *Int. Rev. Neurobiol.* **51**, 325 (2002).
20. A. C. Rego, C. R. Oliveira, *Neurochem. Res.* **28**, 1563 (2003).
21. G. Aliev *et al.*, *Neurol. Res.* **25**, 665 (2003).
22. J. P. Blass, *Neurol. Res.* **25**, 556 (2003).
23. M. P. Mattson, *Int. Rev. Neurobiol.* **53**, 387 (2002).
24. We thank D. Eliezer and T. McGraw for helpful discussions, K. D'Amico and L. Tong for help with data collection at the Advanced Photon Source, and D. Landry for help with the surface plasmon resonance experiment. This work was supported by P50AG08702, AG16736, AG17490, and NS42855 and in part by Speaker's Fund for Biomedical Research and NIH 1K07AG00959. H.W. is a Pew Scholar

of biomedical sciences and a Rita Allen Scholar. The atomic coordinates have been deposited in the Protein Data Bank (PDB accession code 1SO8).

**Supporting Online Material**

[www.sciencemag.org/cgi/content/full/304/5669/448/DC1](http://www.sciencemag.org/cgi/content/full/304/5669/448/DC1)  
SOM Text  
Figs. S1 to S4  
Tables S1 and S2  
References

8 September 2003; accepted 19 March 2004

# Dissociable Roles of Ventral and Dorsal Striatum in Instrumental Conditioning

John O'Doherty,<sup>1\*</sup> Peter Dayan,<sup>2</sup> Johannes Schultz,<sup>1</sup> Ralf Deichmann,<sup>1</sup> Karl Friston,<sup>1</sup> Raymond J. Dolan<sup>1</sup>

Instrumental conditioning studies how animals and humans choose actions appropriate to the affective structure of an environment. According to recent reinforcement learning models, two distinct components are involved: a "critic," which learns to predict future reward, and an "actor," which maintains information about the rewarding outcomes of actions to enable better ones to be chosen more frequently. We scanned human participants with functional magnetic resonance imaging while they engaged in instrumental conditioning. Our results suggest partly dissociable contributions of the ventral and dorsal striatum, with the former corresponding to the critic and the latter corresponding to the actor.

The ability to orient toward specific goals in the environment and control actions flexibly in pursuit of those goals is a hallmark of adaptive behavior. Instrumental conditioning, the most basic form of such behavior, allows an organism to learn contingencies between its own responses and rewarding or punishing outcomes (1–5). Models of reinforcement learning, such as the actor-critic (6) or advantage learning model (7), provide a two-process account of instrumental conditioning. One component, the critic, uses a temporal difference prediction error signal to update successive predictions of future reward associated with being at a state of the external and internal environment (determined by the arrangement of stimuli). The other component, the actor, uses a similar signal to modify stimulus-response or stimulus-response-reward associations in the form of a policy, so that actions associated with greater long-term reward are chosen more frequently on subsequent trials (8–11).

A putative neuronal correlate of these temporal difference prediction error signals is the phasic activity of dopamine neurons (12–

14), which send prominent projections to the ventral and dorsal striatum. Lesion and human imaging studies suggest that the ventral and dorsal striatum may have distinct functions. The former is implicated in reward and motivation (15). The latter is implicated in motor and cognitive control (16–19), specifically the learning of stimulus-response associations. On the basis of these findings, a putative neural substrate for reinforcement learning has been proposed (20), according to which dopaminergic projections to ventral striatum might be involved in reward prediction, corresponding primarily to the critic component of instrumental learning, whereas dopaminergic projections to dorsal striatum might be involved in the modulation of stimulus-response or stimulus-response-reward associations, corresponding to the instrumental actor.

We analyzed functional magnetic resonance imaging (fMRI) data from human participants performing an instrumental conditioning task. We used a reinforcement learning model called advantage learning (21) to calculate a reward prediction error signal and tested for correlations between that signal and evoked neural activity in the striatum. To dissociate stimulus-response learning from value prediction learning itself, we used a yoked Pavlovian conditioning task as a control condition. This task involves the same value predictions (critic), without ac-

tion selections (actor). If the ventral striatum corresponds to the critic, then this region should show prediction error activity during both the instrumental and Pavlovian conditioning tasks. If the dorsal striatum corresponds to the actor, then we would expect it to manifest stronger prediction error-related activity during instrumental than during Pavlovian conditioning.

The instrumental task was composed of two trial types: reward and neutral. In the reward trials, participants had to choose between one of two stimuli: one associated with a high probability of obtaining a juice reward (on 60% of occasions) and the other with a low probability of obtaining a juice reward (on 30% of occasions). In neutral trials, participants had to choose between two other stimuli associated with either a high (60%) or low (30%) probability of obtaining an affectively neutral solution. The Pavlovian task was identical to the instrumental task (with both reward and neutral trials), except that the computer made the selection and the participant's task was to indicate which stimulus had been chosen by the computer (Fig. 1A).

Participants rated the fruit juice as significantly more pleasant than the control tasteless solution in both the instrumental and Pavlovian conditioning tasks ( $P < 0.001$ ; Fig. 1B). In the reward trials of the instrumental task, participants chose the high-probability action significantly more frequently than the low-probability action, but they showed no preference for the high-probability action in the neutral trials (Fig. 1C). There was evidence of "response matching" in the instrumental task (22) in that the ratio of responses made to the high-probability and low-probability stimuli was 1.92:1 during reward trials, a value very close to the actual 2:1 ratio of reward probabilities associated with the two stimuli.

To obtain a behavioral measure of learning in the Pavlovian conditioning task, we tested for differences in reaction times between responses in the reward and neutral trials (pooling over responses to high- and low-probability stimuli) between early and late phases of the session. Participants were faster to respond during the reward trials than during the neutral trials by the second block of trials (Fig. 1D).

<sup>1</sup>Wellcome Department of Imaging Neuroscience, Institute of Neurology, <sup>2</sup>Gatsby Computational Neuroscience Unit, University College London, London WC1N 3BG, UK.

\*To whom correspondence should be addressed. E-mail: j.odoherty@fil.ion.ucl.ac.uk

## Supplementary Online Material

### ABAD Directly Links

#### A $\beta$ to Mitochondrial Toxicity in Alzheimer's Disease

Joyce W. Lustbader, Maurizio Cirilli, Chang Lin, Hong Wei Xu, Kazuhiro Takuma, Ning Wang, Casper Caspersen, Xi Chen, Susan Pollack, Michael Chaney, Fabrizio Trinchese, Shumin Liu, Frank Gunn-Moore, Lih-Fen Lue, Douglas G. Walker, Periannan Kuppusamy, Zay L. Zewier, Ottavio Arancio, David Stern, Shirley ShiDu Yan and Hao Wu

#### Methods

**Text S1: Immunoprecipitation/immunoblotting.** Human brain tissues from AD patients and age-matched non-demented controls (N=3 in each case) were homogenized in Tris buffer (10 mM Tris, 0.1 M NaCl, 1 mM EDTA, 100  $\mu$ g/ml PMSF, 1 $\mu$ g/ml aprotinin), immunoprecipitated with rabbit anti-A $\beta$  IgG (3  $\mu$ l/500  $\mu$ g protein, generously provided by Dr. Steven Younkin, Mayo Clinic, Jacksonville, FL) at 4°C overnight, and Western blotting was done with mouse anti-ABAD IgG (1:1000). Immunoprecipitation was performed on incubation of crude extracts (500  $\mu$ g) from cerebral cortex with anti-A $\beta$  antibody followed by immunoblotting with anti-ABAD IgG. Peroxidase-conjugated goat anti-mouse IgG (specific for heavy chain, Jackson Lab) was used as a secondary antibody. Electrophoresis was performed with 12% Tris-Glycine SDS-PAGE. Results shown are representative of the 3 patients in each group. The same methodology was employed for immunoprecipitation/immunoblotting studies of mitochondria derived from brains of Tg mAPP/ABAD mice.

**Text S2: Transgenic (Tg) mice** overexpressing a mutant human form of amyloid precursor protein (mAPP), the latter a minigene encoding hAPP695, 751 and hAPP770 bearing V717/F, K670M, N671L; J-20 line) in the C57BL6 background were provided by Dr. Lennart Mucke (1). The latter are termed Tg mAPP mice (>N10 in the C57BL/6 strain). Tg ABAD mice (N8 in the C57BL/6 strain), which overexpress ABAD under control of the PDGF B-chain promoter have described previously (2). Tg mAPP and Tg ABAD animals were crossed to generated Tg mAPP/ABAD, Tg mAPP, Tg ABAD and nontransgenic littermates. Offspring were identified by PCR using primers for specific for each transgene.

**Text S3: Isolation of mitochondria.** Brain tissue in isolation buffer (20 mM Hepes at pH 7.2 and 1 mM EDTA) was subjected to 10 strokes of a glass teflon potter homogenizer. The homogenate was centrifuged at 1,700 rpm for 6 min at 4°C. The resulting supernatant was then centrifuged at 5000 g for 10 min. The pellet was resuspended in isolation buffer, and layered on a Ficoll gradient generated from 5 ml of 11% Ficoll and 3 ml of 7.5 % Ficoll and centrifuged in an AH-628 rotor at 79,000g for 30 minutes. The pellet was resuspended again in isolation buffer, incubated with fresh digitonin (1.25 mg/100 mg brain tissues) for 15 min on ice, and then centrifuged at 6,500 rpm for 10 min. The resulting new pellet, containing highly purified mitochondria, was washed with 0.2% BSA and resuspended in isolation buffer.

**Text S4: Crystallography.** Expression and purification of human ABAD was performed as described (2,3). For crystallization, ABAD was concentrated to 10 mg/ml in 25 mM MES at pH 6.0, 0.1 M NaCl and 5 mM DTT and mixed with 5 mM NAD and 3- to 4-fold molar excess of A $\beta$  (residues 1-40; Biosource, CA). The mixture was crystallized by vapor diffusion at 22°C using a precipitant solution containing 0.1 M MES at pH 6.0, 2.5 M NaCl, 5 mM benzamidine and 5 mM NAD. Diffraction data were collected at the COM-CAT beamline of Advanced Photon Source and processed with the HKL package (4). The structure was determined by molecular replacement calculations in the program Replace (5, 6) using the rat ABAD structure as a search model. Limited six-dimensional search and a high large term cutoff (2.0) were used in the structure determination. Retrospectively, these strategies were crucial in overcoming the hurdle provided by the high symmetry of the space group and the large conformational differences between rat ABAD and human A $\beta$ -bound ABAD structures. Refinement was carried out by the simulated annealing protocol in CNS (7). Model building was performed in program O and ribbon diagrams were plotted in program SETOR (8, 9). The final atomic model contains residues 6-94, 114-207 and 229-253.

**Text S5: Studies with ABAD-derived peptides.** ABAD decoy peptide (ABAD-DP, residues 92-120, with a sequence of Ala-Gly-Ile-Ala-Val-Ala-Ser-Lys-Thr-Tyr-Asn-Leu-Lys-Lys-Gly-Gln-Thr-His-Thr-Leu-Glu-Asp-Phe-Gln-Arg-Val-Leu-Asp-Val) and ABAD reverse peptide (ABAD-RP, residues 120-92) were synthesized by Biotechnology Lab at Yale University. For binding studies, ABAD was immobilized on CM5 sensor chip (10). As indicated, A $\beta$ (1-40) or A $\beta$ (1-42) alone or with either ABAD-DP or ABAD-RP (range of concentrations) was injected at a flow rate of 30  $\mu$ l/min for 2 min at 25°C using Biacore X (Pharmacia). The reaction/binding buffer contained 50 mM Hepes at pH 7.4, 0.15 M NaCl, 1 mM EDTA, and 0.005% Tween 20. Data analysis was performed using Biacore X biosensor system (Uppsala, Sweden) and BIA evaluation 3.0 software (Biacore, Sweden). Response data are plotted in Resonance Units versus ABAD peptide concentrations (nM), and were fit to a one-site model for competitive inhibition to obtain the  $K_i$ .

**Text S6: The effect of ABAD-DP on cytochrome c release.** Primary cortical neurons (4 day) from mice of each of the genotypes were cultured (11). The effect of ABAD-DP on cytochrome c release was studied by pre-treating cultures with ABAD-DP (10  $\mu$ M) or ABAD-RP (10  $\mu$ M) for 60 minutes, followed by incubation with A $\beta$ (1-42; 1  $\mu$ M) for nonTg and Tg ABAD mice. After 24 hours at 37°C, cytosolic cytochrome c was determined by the following procedure. Briefly, cells plated on 100 mm dishes were washed with cold PBS, scraped using a rubber policeman, and collected by centrifugation at 300 g for 5 min at 4°C. The pellet was resuspended in 400  $\mu$ l of lysis buffer containing 50 mM Tris at pH 7.4, 1 mM EDTA, 1 mM EGTA, 250 mM sucrose, 2  $\mu$ g/ml leupeptin, 1 mM PMSF, and 1  $\mu$ g/ml pepstatin A and disrupted with 10 strokes of a Dounce homogenizer. Cytosol and membrane fractions were separated by centrifugation at 105,000 g for 1 hour at 4°C (11). The resulting pellets were resuspended in 50  $\mu$ l of lysis buffer and supernatants were concentrated to 20  $\mu$ l. The protein content of each fraction was determined by the BioRad DC protein assay (BioRad Laboratories, Hercules, CA).

Samples (40 µg/lane) were subjected to 12% SDS-PAGE, followed by immunoblotting using anti-cytochrome c antibody (1:500) (Phamergen).

**Text S7: The effect of ABAD-DP on intracellular generation of ROS.** Studies were also performed to determine the effect of ABAD-DP on intracellular generation of ROS by neurons from Tg mice using DCFDA fluorescent probe (12, 13). Cells plated on 100 mm dishes were washed with Hanks balanced saline solution, incubated with 0.05% trypsin-EDTA containing 1 µM DCFDA for 25 minutes and collected by centrifugation at 300 g for 5 min at room temperature. The pellet was resuspended in 1.5 ml Earle's balanced saline solution and exposed to A $\beta$  (1-42, 4 µg/ml) for 5 minutes. Fluorescence was measured with excitation at 490 nm and emission at 530 nm using a FluoroMax-2 spectrofluorometer (Jobin Yvon Inc., Edison, NJ). Other studies investigated the effect of ABAD-DP on A $\beta$ -induced and spontaneous DNA fragmentation (Cell Death Detection ELISA<sup>PLUS</sup>, Roche Diagnostics Co. Indianapolis, IN) and LDH release (sigma).

**Text S8: EPR spectra** were recorded on frozen brain tissues in liquid nitrogen using a quartz dewar at X-band. Brain tissue was extruded in the form of a cylinder with 5 mm diameter at room temperature and quickly frozen in liquid nitrogen. The measurements were performed on frozen intact tissue. No processing (grinding) was done on the frozen sample to avoid artifacts. The spectrometer was set at a frequency of 9.561GHz, a modulation amplitude of 2.5G and a microwave power of 1mW. Spectral acquisitions were performed for 10 min on each sample.

**Text S9: The radial-arm water maze task** (P<0.05; N=7-8) was performed as previously described. Investigators were blinded to mouse genotypes (14). Mice had to find a platform hidden beneath the water surface at the end of one of the six arms. The four groups of animals under study in our behavioral experiments were littermates. This breeding strategy and the C57BL/6 background were employed to enhance the reproducibility and reliability of our results in the radial arm water maze, based on work of other investigators. Time to reach the platform and speed of swimming were recorded and analyzed with a video-tracking system (HVS-2020, HVS Image, UK).

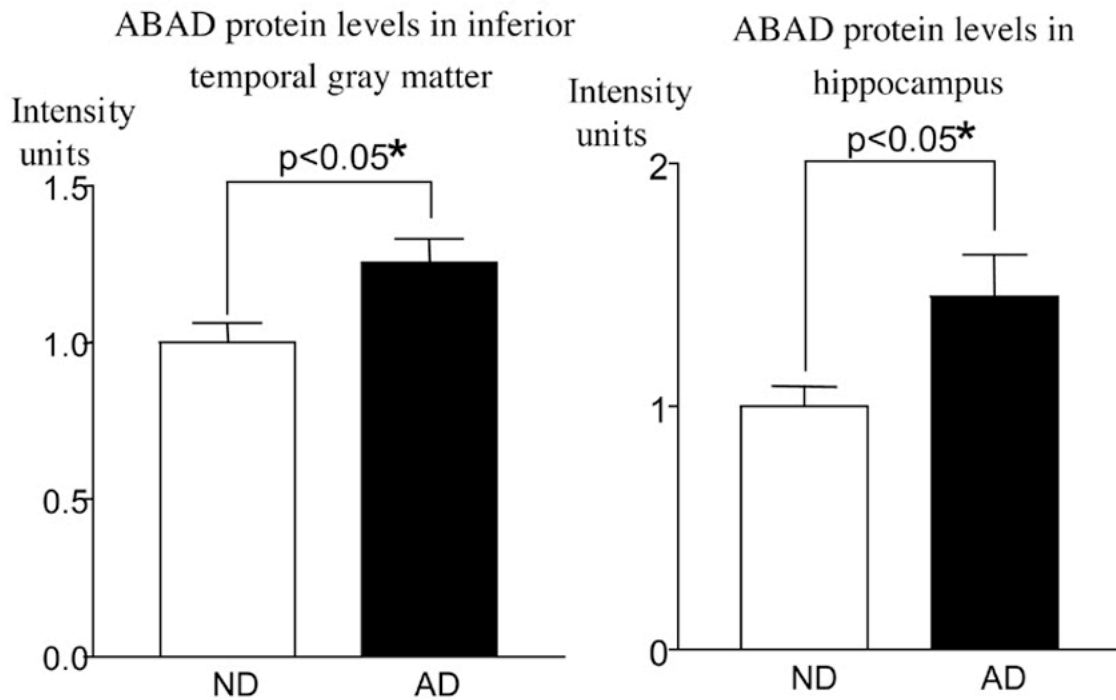


**Figure S1.** Increased expression of ABAD in AD brains (n=19) as compared with age-matched controls (n=15). Brains from age-matched, pathologically confirmed 19 patient with AD (means  $\pm$  age  $85.5 \pm 2.07$ ), and 15 non-demented (ND) patients (means  $\pm$  age  $82.07 \pm 1.465$ ) were harvested according to the rapid autopsy procedure developed at Sun Health Institute (postmortem time  $2.7 \pm 0.306$  and  $2.14 \pm 0.162$  hour, respectively, for AD and ND patients) (15). Two AD-affected brain regions were analysed, inferior temporal lobe grey matter and hippocampus. Protein extracts were prepared by sonication with 5 volumes of extracting buffer (2% SDS, 1mM EDTA, and protease inhibitors in PBS) and 8  $\mu$ g of protein from each brain extract were loaded onto reducing NuPAGE 4-12% Bis-Tris gel (Invitrogen, Carlsbad, CA). Immunoblotting was performed with specific antibodies to ABAD (monoclonal antibody to human, generated in our lab, 1:10,000) or  $\beta$ -actin (1:10,000, Sigma, St. louis, MO). The immunoreactive bands were detected with Super Signal Pico Chemiluminescent substrate (Pierce Chemicals). Densitometry was performed using the Chemilmager 4000 Imaging system (Alpha Innotech, San Leandro, CA) to determine differences in intensity of the ABAD immunoreactive band, which was normalized according to intensity of the  $\beta$ -actin band. Our results demonstrate a significant increase of ABAD protein in the AD-pathology-affected regions (approximately 28% increase in inferior temporal lobe grey matter and 40% in hippocampus) from AD patients versus ND controls. These data are consistent with our previous data (16) demonstrating enhanced expression of ABAD in AD brain by immunoblotting with anti-ABAD antibody. In contrast, protein extracts prepared from the cerebellum, a region spared from the AD pathology, showed no significant differences between AD patient and ND controls.

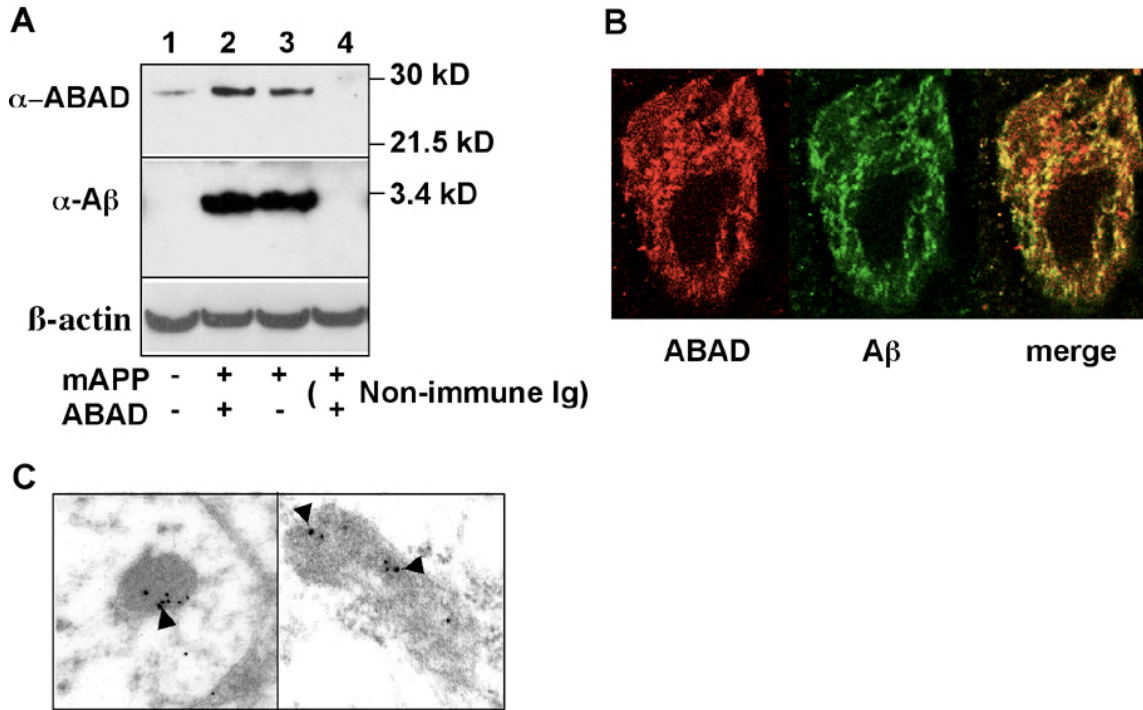


**Figure S2.** Demonstration of ABAD-A $\beta$  complex in brains of Tg mAPP/ABAD mice. A, Co-immunoprecipitation of ABAD and A $\beta$  from mitochondria of transgenic mice. Mitochondrial fractions (500  $\mu$ g) from cerebral cortex of nonTg, Tg mAPP and Tg mAPP/ABAD mice were immunoprecipitated with mouse anti-A $\beta$  IgG (6E10; 8  $\mu$ g/ml), or nonimmune IgG (8  $\mu$ g/ml) at 4°C overnight followed by Western blotting with mouse anti-ABAD (1:10,000). The middle panel shows total input protein reprobed with anti-A $\beta$  antibody (6E 10). Lower panel shows immunoblotting of  $\beta$ -actin for crude extracts from mouse brains. B, Co-localization of ABAD and A $\beta$  in the brain of a Tg mAPP/ABAD mouse using confocal microscopy with antibodies to ABAD (red) and A $\beta$  (green) (magnification 300-fold). C, Colocalization of ABAD and A $\beta$  in mitochondria of brains from Tg mAPP /ABAD mouse using electron microscopy. Double immunogold staining was performed with rabbit anti-A $\beta$  IgG and mouse anti-ABAD IgG followed by goat anti-rabbit IgG conjugated to 12 nm gold particles (for A $\beta$ 1-42) and goat anti-mouse IgG conjugated to 18 nM gold particles (for ABAD). Arrowheads depict gold particles localizing ABAD antigen. The smaller gold particles represent sites of localization of A $\beta$ .

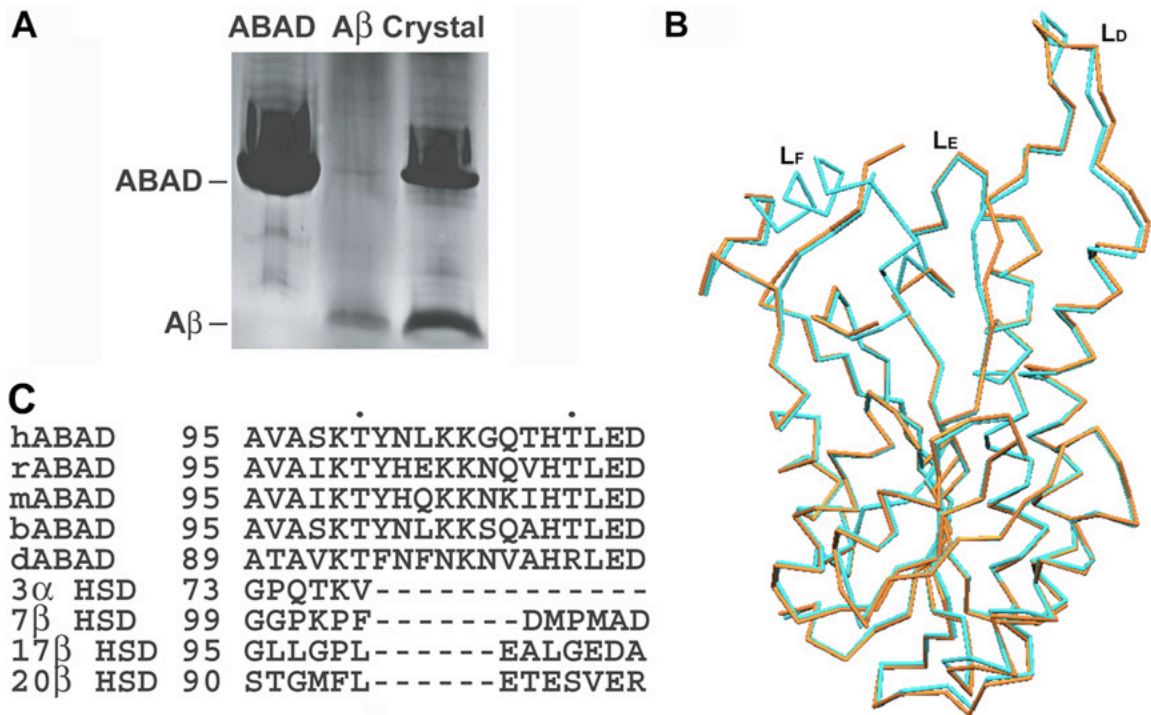


**Figure S3.** A, SDS-PAGE of washed and dissolved crystals of human ABAD and A $\beta$ . Lanes from left to right: ABAD standard, A $\beta$  (1-40) standard and dissolved crystals. B, Superposition of rat ABAD in complex with NAD (orange) and human ABAD in complex with NAD and an inhibitor (cyan). The L<sub>D</sub> and L<sub>E</sub> loops are very similar. The L<sub>F</sub> loop is ordered in the human structure but disordered in the rat structure. C, Sequence alignment of the disordered part of the L<sub>D</sub> loop (residues 95-113) among human, rat, mouse, bovine and *Drosophila* ABAD and several HSDs, members of the SDRs, showing the insertion in ABAD relative to other HSDs.

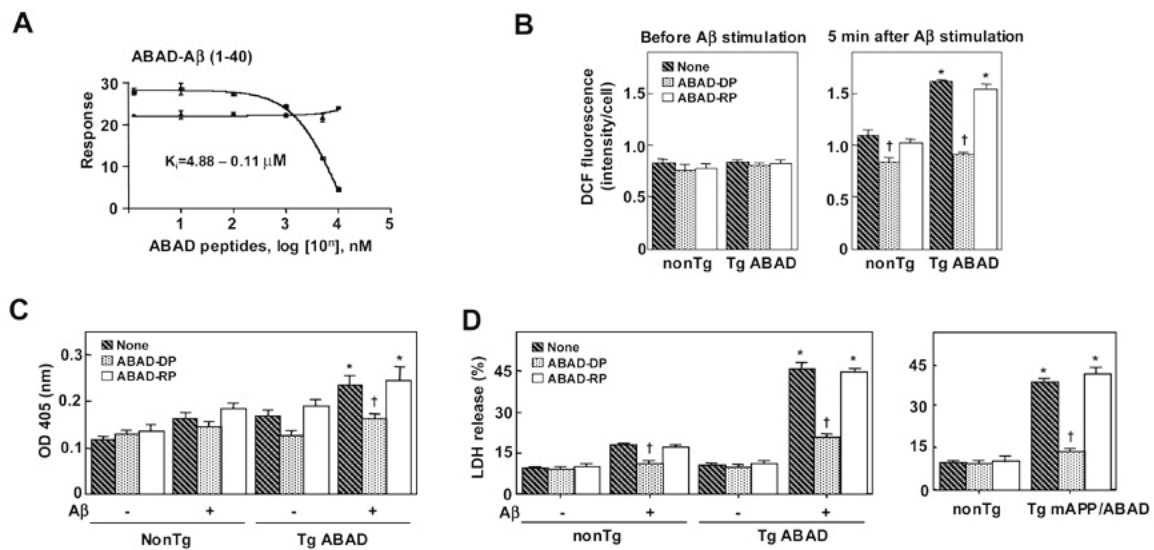


**Figure S4.** A, Inhibition of ABAD-A $\beta$  (1-40) interaction by ABAD-DP. ABAD was immobilized on the sensor chip of the Biacore and A $\beta$  (1-40), in the presence of the indicated concentrations of ABAD-DP or ABAD-RP, was in the mobile phase. Response data are plotted in Resonance Units versus ABAD peptide concentrations (nM). B-D, Inhibition of A $\beta$ -induced generation of ROS (B), DNA fragmentation (C) and LDH release (D) by ABAD-DP, but not by ABAD-RP. For inhibition by ABAD peptides, cells were pre-incubated with ABAD-DP or ABAD-RP (10  $\mu\text{M}$ ) for 60 min before A $\beta$  treatment. \* $P < 0.05$ , versus nonTg cells; † $P < 0.05$ , versus without ABAD-DP treatment.

**Table S1.** Crystallographic statistics.

Crystals of the ABAD/A $\beta$ complex	
Space group	P432
Cell dimensions	a=130.0Å
Diffraction Data	
Resolution	30-2.3Å
R <sub>sym</sub> (last shell)	5.1% (15.2%)
Completeness (last shell)	99.8% (99.8%)
I/SigI (last shell)	57.7 (13.0)
Molecular Replacement	
Resolution	10-4.0Å
Number of rotations searched	181
Correlation coefficient	32.4%
R	44.3%
Refinement	
Resolution	30-2.3Å
Sigma cutoff	0.0
Number of protein residues	208
Number of protein atoms	1480
Number of solvent and ion atoms	121
Number of reflections used	17049
R (R <sub>free</sub> )	23.1% (26.1%)
RMSD bond length	0.006Å
RMSD bond angle	1.1°

**Table S2.** ABAD interaction.

Peptide	K <sub>d</sub> (nM)
A $\beta$ 1-40	38.4 ± 4.6
A $\beta$ 1-42	55.8 ± 10.9
A $\beta$ 1-20	88.9 ± 19.9
A $\beta$ 25-35	> 10 <sup>3</sup>
PrP 109-141	> 10 <sup>6</sup>
Amylin	> 10 <sup>7</sup>

\*These studies were performed by immobilizing the indicated amyloid-related peptide on microtiter wells followed by blocking excess sites in the well, and then doing a binding assay by addition of fluorescein-labeled ABAD. Similar results were obtained using a radioligand binding assay (<sup>125</sup>I-labeled ABAD).

## References

1. L. Mucke *et al.*, *J Neurosci* **20**, 4050-8 (2000).
2. S. D. Yan *et al.*, *J Biol Chem* **275**, 27100-9 (2000).
3. S. D. Yan *et al.*, *J Biol Chem* **274**, 2145-56 (1999).

4. H. K. Anandatheerthavarada, G. Biswas, M. A. Robin, N. G. Avadhani, *J Cell Biol* **161**, 41-54 (2003).
5. Z. Otwinowski, W. Minor, *Methods Enzymol.* **276**, 307-326 (1997).
6. L. Tong, *J. Appl. Cryst.* **26**, 748-751 (1993).
7. A. T. Brunger *et al.*, *Acta Crystallogr.* **D54**, 905-21 (1998).
8. T. A. Jones, J.-Y. Zou, S. W. Cowan, M. Kjeldgaard, *Acta Crystallogr.* **A47**, 110-119 (1991).
9. S. V. Evans, *J. Mol. Graph.* **11**, 134-8 (1993).
10. T. Valdes-Gonzalez, J. Inagawa, T. Ido, *Peptides* **22**, 1099-106 (2001).
11. K. Takuma *et al.*, *J Biol Chem* **276**, 48093-9 (2001).
12. J. P. Crow, *Nitric Oxide: Biology and Chemistry* **1**, 145-157 (1997).
13. N. W. Kooy, J. A. Royall, H. Ischiropoulos, *Free Radic Res* **27**, 245-54 (1997).
14. G. Di Rosa, T. Odrijin, R. A. Nixon, O. Arancio, *J Mol Neurosci* **19**, 135-41 (2002).
15. L. F. Lue *et al.*, *Experimental Neurology* **171**, 29-45 (2001).
16. S. D. Yan *et al.*, *Nature* **389**, 689-695 (1997).